Electron Nuclear Double Resonance Spectroscopy

Raymond S. Eachus and Myra T. Olm

Summary. Precise information about the molecular structure, stereochemistry, and environment of paramagnetic species can be obtained by electron nuclear double resonance (ENDOR) spectroscopy. This technique has been applied in a wide range of disciplines to liquid-phase, single-crystal, and powder samples. In some cases—the study of defects in ionic single crystals, for instance—the volume and complexity of data obtained by ENDOR can hinder interpretation. Such difficulties have been overcome by the use of supplemental ENDOR techniques that simplify the assignment of ENDOR lines. The increased use of computers for the automation of instrumentation, the design of experiments, and the analysis of data has made possible the study of a wider range of problems. With these improvements, as well as with the increased sensitivity provided by optically detected ENDOR, it is now feasible to study polycrystalline and amorphous materials, such as thin-film semiconductors and biological samples in vivo.

Electron nuclear double resonance (ENDOR) spectroscopy is a magnetic resonance technique that can provide detailed information about the structure and composition of paramagnetic systems and is currently used to study problems in biology, chemistry, geology, mineralogy, and physics. This article presents an overview of ENDOR and its applications. Examples of liquid-phase, single-crystal, and powder studies are used to illustrate the types of information that can be obtained and experimental problems commonly encountered.

ENDOR Spectroscopy

In ENDOR spectroscopy, the effect of radio-frequency (rf) excitation on the intensity of electron spin resonance (ESR) signals is monitored, thereby performing simultaneous nuclear magnetic resonance (NMR) and ESR experiments. ENDOR combines the inherent sensitivity of ESR with the capability of NMR to provide structural information at the molecular level. Thus, any description of ENDOR begins with discussions of both ESR and NMR.

In an ESR experiment, the energy required to change the orientation of an unpaired electron's spin relative to the direction of an applied d-c magnetic field, B_0, is measured. Such experiments, therefore, are limited to paramagnetic systems. ESR data are obtained in the form of a g tensor (**g**), which describes the electronic Zeeman interaction between the B_0 field and the electron spin; a hyperfine tensor (**A**) resulting from magnetic coupling between the unpaired electron and neighboring nuclear spins; and a zero-field tensor (**D**) associated with interelectronic interactions.

Sometimes it is also possible to derive a quadrupole interaction tensor (**Q**), which is nonzero for nuclei with spin $I > 1/2$ and results from the interaction of the nuclear spin with the electric-field gradient at the nucleus. This tensor is sensitive, therefore, to the total charge distribution surrounding the nucleus. **A** and **g** reveal information about the elemental composition of the paramagnetic species, its geometry and environment, and the distribution of the unpaired electron within a molecular framework. The geometrical relationships that exist between the diagonal components of **A** and **g** and external reference frames, such as the axes of a host crystal, can provide important additional structural information.

The hyperfine interaction can be a particularly rich source of structural data. This information is deduced from the line splittings in the ESR spectrum. If the unpaired electron is highly delocalized, however, interactions with many nuclei can broaden the ESR spectrum, with a concomitant loss of detail. It may be possible to retrieve such data by using ENDOR; in effect, ENDOR extends the resolution of the ESR experiment.

To see how the magnetic resonance parameters can be derived from ESR and ENDOR spectra, it is useful to consider the energy-level diagram for a simple system of one unpaired electron with spin $S = 1/2$ interacting with a single nucleus with spin $I = 1/2$ presented in Fig. 1. This diagram shows the effects of the electronic Zeeman interaction ($g_e\mu_B B_0$), the hyperfine interaction ($1/2A$, where A is the principal component of the hyperfine tensor **A**), and the nuclear Zeeman interaction ($g_N\mu_N B_0$) on the electronic energy levels in an applied magnetic field of magnitude B_0. (The nuclear Zeeman term results from the interaction of the nuclear spin with B_0.) The parameters μ_B and μ_N are the Bohr and nuclear magnetons, respectively.

In the ESR experiment, transitions are induced between levels 1 and 4 and between levels 2 and 3, processes that fulfill the selection rules $\Delta m_S = \pm 1$, $\Delta m_I = 0$. The two transition energies are given by

$$\Delta E_{\mathrm{ESR}} = h\nu = g_\theta \mu_B B_0 \pm \frac{1}{2} A_\theta \qquad (1)$$

where the subscript θ denotes the angular dependence of ESR lines, which is related to the symmetry of the specific system and its orientation within an arbitrary laboratory reference frame. Transitions between levels 1 and 2 and levels 3 and 4 obey the selection rules $\Delta m_S = 0$ and $\Delta m_I = \pm 1$ and are formally forbidden in ESR, but they are the basis of both NMR and ENDOR experiments. The energies of the ENDOR transitions are given, to first order, by

$$\Delta E_{\mathrm{ENDOR}} = h\nu = \left| \frac{A}{2} \pm g_N \mu_N B_0 \right| \qquad (2)$$

In an ESR experiment, the paramagnetic sample is placed in the d-c magnetic field, B_0, which is of the order of 1 to 20 kilogauss, and irradiated with a microwave field, B_1, of frequency ν_1 oriented perpendicular to B_0. It is convenient to keep the frequency of B_1 fixed and to vary B_0 until an electronic spin-flip transition ($1 \rightarrow 4$ or $2 \rightarrow 3$ in Fig. 1) is induced by absorption of energy from B_1. The microwave field is sustained in a resonant cavity structure; placed between the pole gaps of the direct-current (d-c) magnet, which is designed to maximize B_1 at the sample; the change in the microwave energy stored in the cavity is monitored as B_0 is varied. The ESR

R. S. Eachus and M. T. Olm are members of the Chemistry Division of the Research Laboratories, Eastman Kodak Company, Rochester, New York 14650.

spectral lines are observed at values of B_0 that correspond to the transition energies given in Eq. 1.

In an ENDOR experiment, the paramagnetic sample is placed in a static magnetic field, B_0, selected so that it is centered on an ESR transition. The ESR signal intensity at this field value is then monitored as the sample is irradiated with high levels of the fixed microwave field, B_1. This tends to equalize the populations of the electronic spin levels associated with the ESR transition; that is, to "saturate" the ESR signal. An rf field, B_2, of varying frequency, ν_2, is then introduced through metal coils inserted into the microwave cavity (Fig. 2).

When ν_2 satisfies Eq. 2, an ENDOR transition is induced. This tends to desaturate the ESR signal so that the ENDOR transition is detected by a change in the intensity of the ESR signal at B_0. The ENDOR spectrum consists of two lines, either centered at $A/2$ and separated by $2g_N\mu_N B_0$, if $A/2 > g_N\mu_N B_0$, or centered at $g_N\mu_N B_0$ and separated by A, if $A/2 < g_N\mu_N B_0$. If there are no quadrupole interactions and no major second-order effects (such as spin-spin coupling between nuclei), the ENDOR spectrum will consist of pairs of lines corresponding to each different kind of nucleus. ENDOR transition energies usually can be calculated for each nucleus independently; thus, Eq. 2 is applicable, to the first order, in systems more complex than those represented by the four-level scheme in Fig. 1. The ENDOR spectrum will also "fingerprint" the types of interacting nuclei because of the dependence of the transition energy on $g_N\mu_N$.

The intensity of the ENDOR signal, resulting from the simultaneous absorption of microwave and rf radiations, depends on the delicate balance between the excitation rates resulting from B_1 and B_2 and the competing electronic and nuclear spin-relaxation rates. In practice, ENDOR signal intensities are one-tenth to one-hundredth of the corresponding ESR signal.

A more thorough treatment of the theory, history, and practical details of ENDOR is available in the general literature (*1, 2*) and in the specific references cited here. Annual reviews of the pertinent literature can also be found in the specialist periodical reports published by the Royal Society of Chemistry (*3*).

Liquid-Phase ENDOR Studies

The simplest application of ENDOR is to the study of radicals in solution, where rapid molecular motion averages out the angular dependencies of $\mathbf{g}$, $\mathbf{A}$, $\mathbf{D}$, and $\mathbf{Q}$. Solution ENDOR has been used in organic chemistry and the biosciences to facilitate the identification of radicals and to study the solution dynamics of large molecules. The chief advantage of solution ENDOR is its ability to simplify the assignment of complex ESR spectra. This is particularly true for asymmetric organic molecules, in which many magnetic nuclei are not equivalent and thus the ESR spectra are complex.

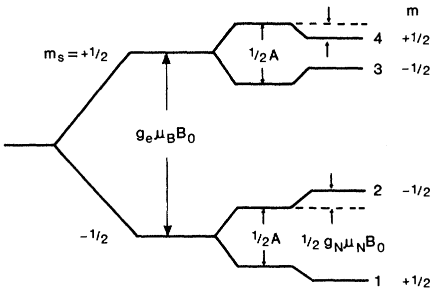

Fig. 1. Energy-level diagram for a four-level spin system with positive A and $A > 2g_N\mu_N B_0$.

Figure 3 shows a typical example of a solution problem in organic chemistry. ESR and ENDOR spectra were obtained from the *N*-phenylbenzophenone imine radical anion in tetrahydrofuran. The ESR spectrum consists of 54 lines, an unexpectedly small number considering that the radical anion contains 15 protons (I = 1/2) and a single nitrogen nucleus (I = 3/2). With significant delocalization of the unpaired electron over the whole molecular framework, more than 4000 ESR lines could result.

The ENDOR spectrum in Fig. 3b was obtained by setting B_0 on one of the 54 ESR signals. Hyperfine interactions with three sets of inequivalent protons were detected as three pairs of ENDOR lines. They were centered at the free-proton frequency, and their separations gave the hyperfine splittings. The hyperfine datum for the single nitrogen nucleus could be obtained by sweeping the region centered at the free-nitrogen nuclear frequency of about 1 megahertz. ESR spectra simulated from the ENDOR data showed that the unpaired electron is not delocalized throughout the radical anion. It is confined to the unique phenyl ring, and the 54 ESR lines result from hyperfine interactions with pairs of *ortho* and *meta* protons, a single *para* proton, and the central nitrogen nucleus.

Although the interpretation of solution ENDOR spectra may be straightforward, it is sometimes difficult to achieve the experimental conditions required to obtain liquid-phase spectra because the fast electronic and nuclear relaxation rates that exist in solution require the use of high microwave and rf powers. These relaxation rates are affected by the radical concentration, the nature of the solvent, and the concentration of impurities, especially water and dissolved oxygen. Furthermore, the relaxation characteristics of each nucleus will depend on the chemical composition and viscosity of the solvent and on its molecular environment.

It is not uncommon, therefore, to have totally different sets of optimum operating conditions for nuclei of the same type in different parts of a molecule. This means that an empirical approach to optimizing the experimental parameters can lead to a low success rate in obtaining complete solution ENDOR data (*4*).

Plato and his colleagues (*5*) took a rigorous approach to this problem, using a density-matrix method (*6*) for calculating ENDOR signal amplitudes as functions of B_1, B_2, temperature, spin concentration, and modulation conditions. One interesting result of such calculations is the prediction that, with the instrumentation presently available, it will be impossible to observe solution ENDOR from certain nuclei, such as ^{17}O, ^{33}S, ^{35}Cl, and ^{37}Cl.

In many organic liquid-phase systems, the ENDOR signal intensity is limited by fast nuclear relaxation rates. In such cases the technique of special-triple ENDOR (ST-ENDOR) can be usefully applied (*7*). Two rf fields are used to excite simultaneously the ENDOR transitions corresponding to a pair of ENDOR lines. At sufficiently strong rf fields, the ENDOR line intensities are independent of relaxation rates and are proportional to the number of nuclei giving rise to the transitions, just as in NMR. Smaller line widths and larger signal intensities are obtained for a given rf power level in ST-ENDOR than in conventional ENDOR.

Single-Crystal ENDOR Studies

The power of the ENDOR technique is most evident in studies of single crystals in which the angular dependencies of the ENDOR lines aid assignment and can be translated into detailed information about molecular structure. The primary experimental problems with single-crystal ENDOR studies are the time and the resources needed to obtain a complete data set.

Even in ionic crystals, in which delocalization of the electron spin onto ions surrounding the paramagnetic center is minimized, the resolution provided by ENDOR gives such a wealth of convoluted structural information that acquisition, assignment, and analysis can take months or years. Only recently has the

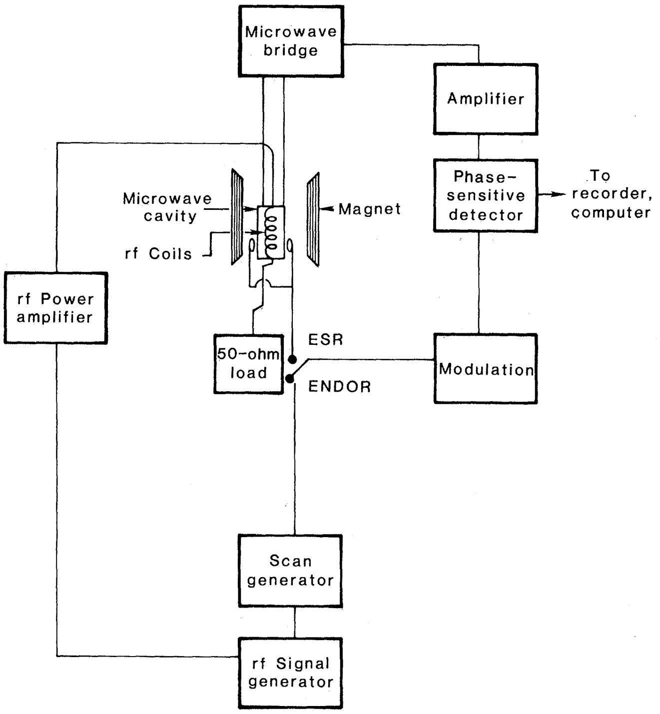

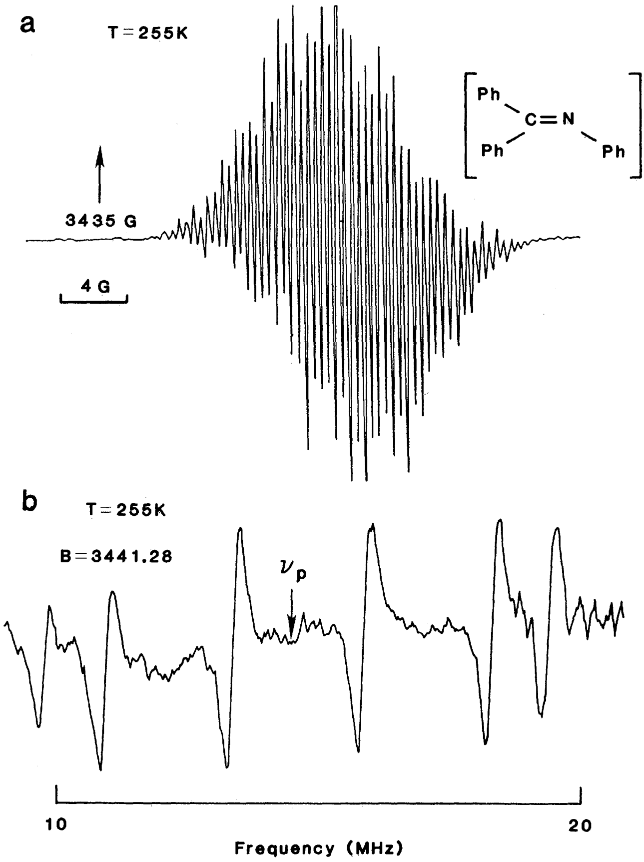

Fig. 2 (left). General block diagram of an ESR-ENDOR spectrometer. Fig. 3 (right). (a) Solution ESR spectrum and (b) solution ENDOR spectrum of the radical anion of *N*-phenylbenzophenone imine above a K-Na alloy suspension in tetrahydrofuran.

increased use of automation and computers made a broad range of structural problems tractable (*8, 9*).

Studies of singlet and triplet states in organic and biological single-crystal systems have been reviewed extensively (*1–3*). Here, we have chosen a problem from inorganic chemistry and photographic science as an example of a single-crystal ENDOR study: elucidation of the structure of the primary divalent rhodium center produced by photolysis of a silver chloride crystal doped with Rh^{3+} cations (*10*).

Transition-metal dopant ions modify the photochemical properties of silver halides, the basic ingredients of photographic film and paper (*11*). They are generally divalent or trivalent and replace lattice Ag^+ ions when doped into AgCl or AgBr, both of which have the NaCl cubic crystal structure. To compensate for their excess positive charge, the dopants form complexes with lattice defects, usually silver ion vacancies. The structure of such a complex determines its photographic behavior and is of both practical and theoretical interest.

Figure 4a shows an ESR spectrum obtained from a single crystal of Rh^{3+}-doped AgCl that was exposed to blue light. The spectrum was measured with B_0 aligned parallel to the <100> axis of the crystal. It consists of three sets of signals from Rh^{2+} species that are structurally equivalent but geometrically inequivalent, which means they differ only by their orientation with respect to B_0. The hyperfine structure in Fig. 4a results from the interaction between the unpaired electron primarily localized on the Rh^{2+} ion, and the nuclei of two Cl^- ligands. These nuclei are directly adjacent to Rh^{2+} but are axially opposed to each other. The resultant Cl^-–Rh^{2+}–Cl^- axis is defined as the z direction of the complex.

Figure 4b shows an ENDOR spectrum obtained with B_0 set to select ESR transitions from complexes oriented with the static magnetic field along the x and y directions. The rf range swept by B_2 in the figure produces primarily ENDOR signals from the two major chlorine nuclei observed by ESR.

The spectrum is complicated. The density of ENDOR signals is increased by the resolution of lines from the two naturally occurring chlorine isotopes (^{35}Cl, 75.77 percent; ^{37}Cl, 24.23 percent) and the multiplicity resulting from the simultaneous excitation of transitions in two geometrically inequivalent complexes. Each ENDOR line is split into three by the quadrupole interaction, which obtains because $I = 3/2$ for both chlorine isotopes. Finally, the lines are further split as a result of indirect spin-spin coupling between isotopically equivalent pairs of axial chlorine nuclei, a process analogous to the nuclear spin-spin coupling observed in NMR.

To interpret this ENDOR spectrum, obtained in a narrow frequency region, we must label each line with a supplemental experimental parameter. In this study the additional information is the behavior of the ENDOR line as θ, the angle between B_0 and the z axis, is varied systematically. This geometrical information allows one to deduce the structure of the complex and defines its orientation relative to the crystal host lattice.

Figure 4c is a plot of the data obtained for two of the geometrically inequivalent Rh^{2+} sites from a rotation study in the (100) plane of AgCl. This plot of ENDOR transition frequency and signal intensity (proportional to dot size) as a function of θ covers the frequency range for transitions from the two axial chlorine nuclei and lower frequencies at which ENDOR signals characteristic of weaker hyperfine interactions with secondary nuclei can be detected. These include the four chlorine nuclei in the equatorial plane of the Cl^-–Rh^{2+}–Cl^- moiety, the central rhodium nucleus, and nuclei from Ag^+ ions in the second and fourth ligand shells. An expansion of the low-frequency region in Fig. 4c would show a wealth of angular data, which could be assigned

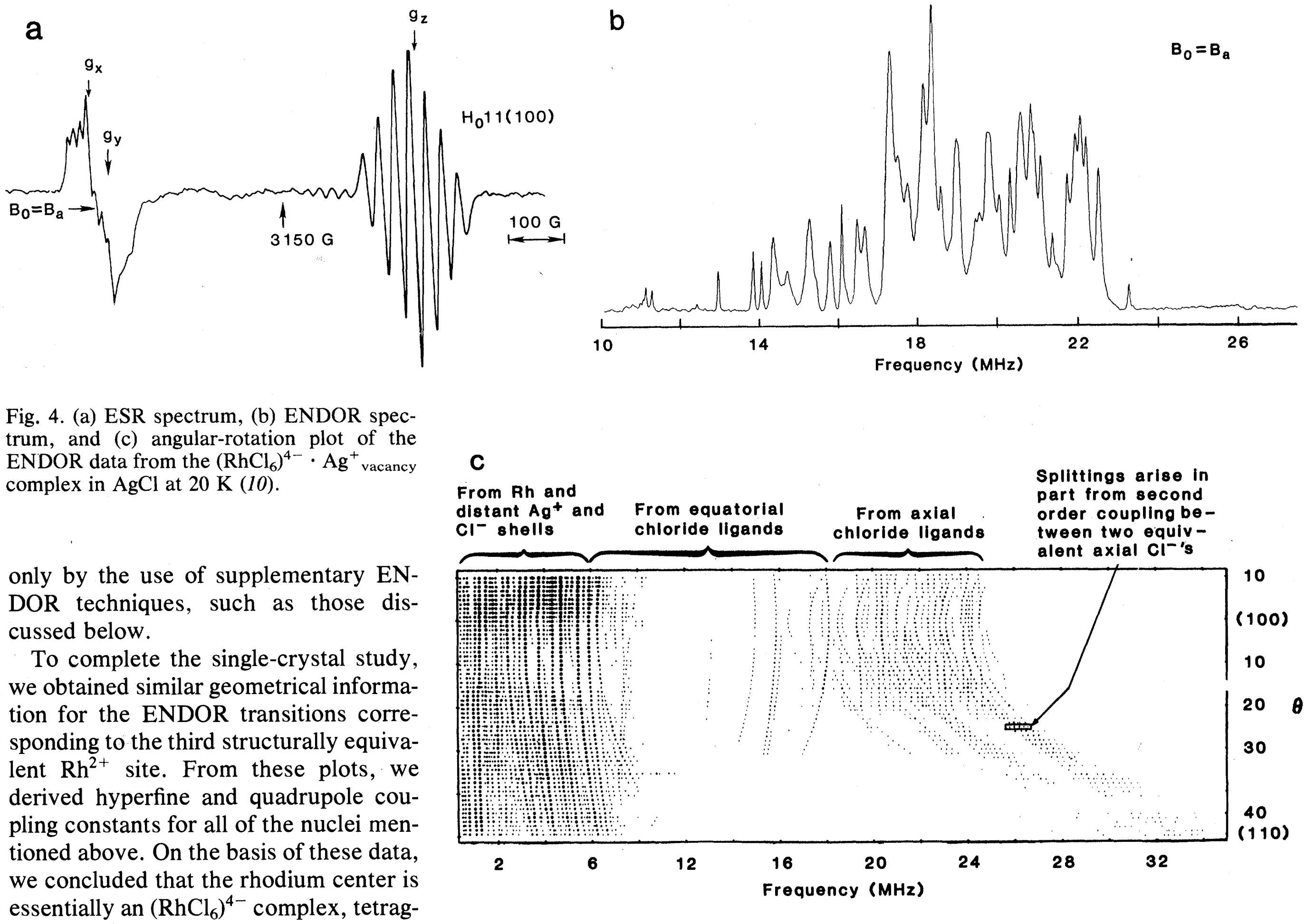

Fig. 4. (a) ESR spectrum, (b) ENDOR spectrum, and (c) angular-rotation plot of the ENDOR data from the $(RhCl_6)^{4-} \cdot Ag^+{}_{vacancy}$ complex in AgCl at 20 K (*10*).

only by the use of supplementary ENDOR techniques, such as those discussed below.

To complete the single-crystal study, we obtained similar geometrical information for the ENDOR transitions corresponding to the third structurally equivalent Rh^{2+} site. From these plots, we derived hyperfine and quadrupole coupling constants for all of the nuclei mentioned above. On the basis of these data, we concluded that the rhodium center is essentially an $(RhCl_6)^{4-}$ complex, tetragonally elongated along the z axis, which is coincident with a <100>, <010>, or <001> crystal direction. The unpaired electron occupies a molecular orbital, composed primarily of the rhodium $4d_{3z^2-r^2}$ orbital, and a charge-compensating Ag^+ vacancy is associated in a next-nearest-neighbor position. There is significant unpaired-electron density delocalized on ligands out to the fourth shell, reflecting the partial covalent character typical of the silver halides.

The interpretation of complex ENDOR spectra can be facilitated by the use of supplemental techniques that reduce the number of, or effectively "label," the ENDOR lines (Fig. 5). One such technique, general triple ENDOR (GT-ENDOR), is related to ST-ENDOR in that two rf fields are applied simultaneously to the sample (*12*). The ENDOR spectrum is swept with the primary rf field, B_2, while a second nonsweeping rf field, B_3, of frequency ν_3 is applied. This frequency, ν_3, is selected to excite a specific ENDOR transition.

In general, all ENDOR transitions in the same electronic manifold [characterized by the same m_S value (Fig. 1)] as that saturated by B_3 will decrease in intensity, whereas those in other manifolds will increase. This fact can be used to determine the relative signs of hyperfine coupling constants for nuclei in the same complex. In addition, this method can be used to separate overlapping ENDOR spectra from different complexes because only signals from the species whose ENDOR transition is stimulated by ν_3 will be affected.

GT-ENDOR was used in the Rh^{2+} study to separate spectra from complexes with different combinations of chlorine isotopes in the principal Cl^-–Rh^{2+}–Cl^- unit (Fig. 5b). One problem with this method is that the GT-ENDOR signal is invariably weaker than the conventional ENDOR spectrum.

Overlapping ENDOR or ESR spectra can also be distinguished by using ENDOR-induced ESR (*13*), a technique that is the converse of the ENDOR experiment. Here, one of the ENDOR transitions is saturated with a fixed B_2 rf field while the B_0 magnetic field is swept. The ENDOR signal intensity will increase whenever an associated ESR transition is induced. Thus, the ESR spectrum associated with the ENDOR transition is obtained. If, as in the rhodium example above, quadrupole transitions are resolved in ENDOR from the nuclei that have resolved hyperfine transitions in the ESR spectrum, relative signs for the major components of the **A** and **Q** tensors can be determined (*14*). This information can then be used to map the overall charge distribution in the complex and to confirm the valence states of the ions involved.

Powder ENDOR Studies

Single crystals of many compounds, such as complex biological molecules, are not available. When studies of frozen glasses or powder samples are unavoidable, important structural information can still be obtained. In a powder sample, the paramagnetic molecules are randomly oriented with respect to the direction of B_0. ENDOR spectra obtained from powders can be of two types, each of which has advantages and disadvantages for interpretation.

The first type is a true powder-pattern spectrum similar to those derived from conventional ESR and NMR experiments on polycrystalline samples. If the ESR spectra from the individual molecules in the sample overlap sufficiently, all of the molecules in the ensemble will be saturated simultaneously during the ENDOR experiment so that a true powder-pattern ENDOR spectrum will be obtained.

The intensity of the powder ENDOR spectrum will be greatest at the two or three frequencies of the rf field B_2 that correspond to the principal values of the hyperfine tensor, but there will be absorptions occurring continuously between these extremes. This frequency spreading of the ENDOR information can broaden the lines, and, if a hyperfine interaction is large and anisotropic, the spectrum will be weak.

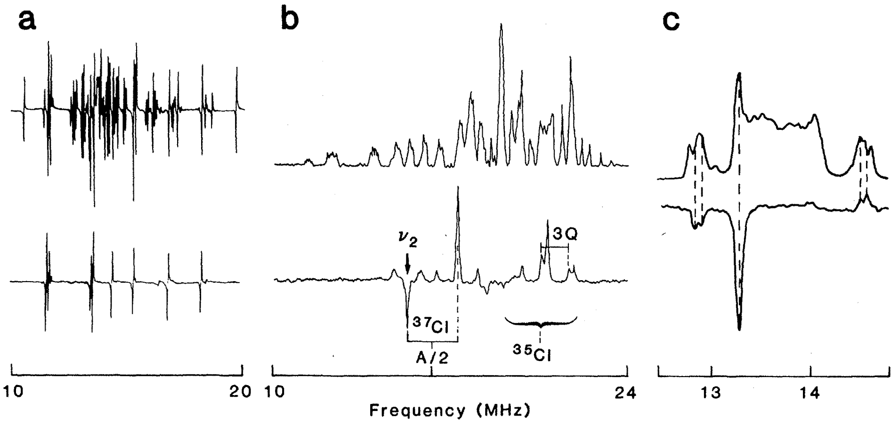

Fig. 5. Comparison of ENDOR and supplementary ENDOR techniques. (a) ENDOR spectrum (top) and CP-ENDOR (right-handed) spectrum (bottom) of a single crystal of Cu^{2+}-doped Zn (bipyam)$_2$(ClO$_4$)$_2$ [bipyam is Bis(2-aminoethyl)amine(di-2-pyridylamine)] in which only the ^{14}N transitions with $m_s = +1/2$ are observed (from four inequivalent nitrogens) [(*29*), courtesy of Taylor and Francis, Ltd.]. (b) ENDOR spectrum (top) and GT-ENDOR spectrum (bottom) of axial chlorine transitions in a rhodium-doped AgCl single crystal in which some of the quadrupole transitions of the ^{35}Cl$^-$–Rh^{2+}–^{37}Cl$^-$ centers are excited (*10*); and (c) ENDOR spectrum (top) and PM-ENDOR spectrum (bottom) of a Cu^{2+}-doped Mg(NH$_4$)$_2$(SO$_4$)$_2$ · H$_2$O single crystal showing the proton transitions and the suppression of the proton-matrix ENDOR line [(*30*), courtesy of Academic Press].

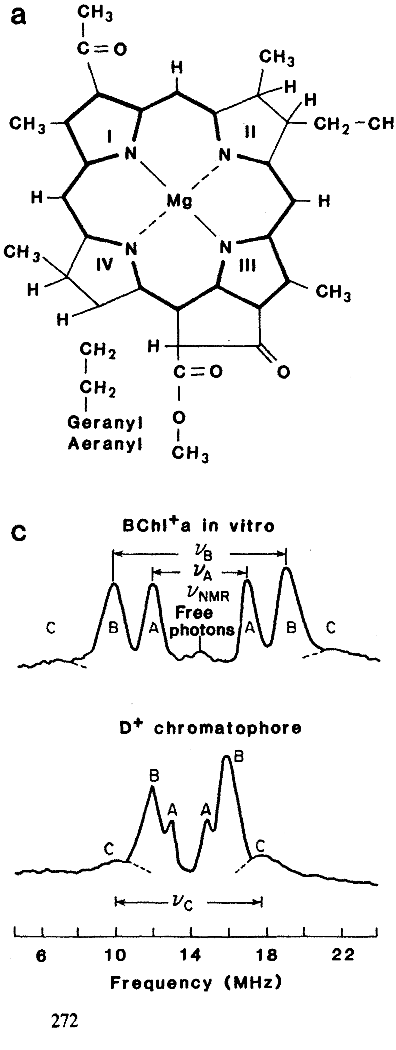

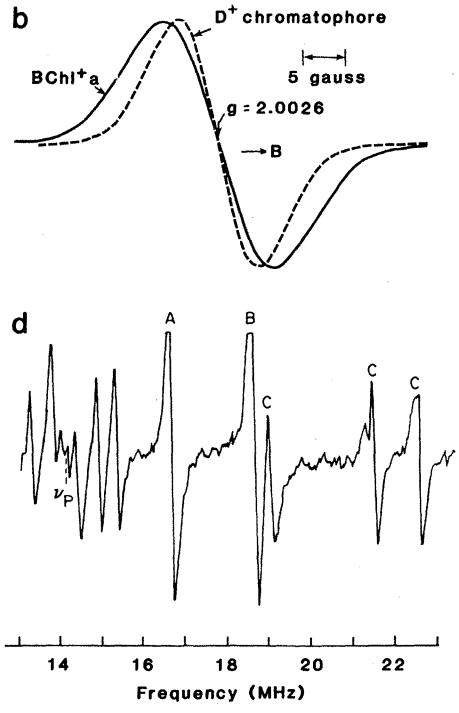

Fig. 6. (a) Structure of the bacteriochlorophyll a molecule. (b) ESR spectra and (c) ENDOR spectra of D$^+$ chromatophore in vivo and BChl$^+$ a cation in vitro at 77 K. (d) Solution ENDOR spectrum of BChl$^+$ a cation at 212 K [(*18*), courtesy of Springer-Verlag].

Spectral resolution and sensitivity can vary for signals corresponding to different nuclei in the same molecule, and transition probabilities and relaxation rates can depend on orientation. Therefore, an incomplete set of ENDOR data may result, making an unequivocal structural assignment difficult. If one has a reasonable idea of the identity of the species and can estimate relaxation characteristics, these problems can be overcome by the use of computer simulation techniques to generate theoretical powder ENDOR spectra for comparison with experiment (*15*).

The second type of powder ENDOR spectrum, usually obtained from samples in which some anisotropy in either **g** or **A** is resolved by ESR, can provide angular information of the type obtained in single-crystal studies. In this case, only part of the molecular ensemble is saturated during the ENDOR experiment. Therefore, only molecules with the specific orientations that produce ESR signals at the selected B_0 value will contribute to the ENDOR spectrum. Some angular information can be obtained from these spectra, because as B_0 is changed, molecules with different orientations contribute to the spectra. In an ideal case the relative orientations of **g** and **A** can be deduced, but their geometrical relationships to the crystal axes remain undetermined. The increased use of computers (*16, 17*) and the supplementary ENDOR techniques discussed below should facilitate analyses of such spectra.

As an example of an application of powder ENDOR, we have selected a problem from biochemistry—the study of light-induced reactions in photosynthetic bacteria (*18*). The ESR signal from the primary donor in purple nonsulfur bacteria, the D$^+$ chromatophore, produced by exposure in vivo, is a single Gaussian line with a linewidth (ΔB) at room temperature of 9.4 ± 0.2 gauss and a *g* value of 2.0026 ± 0.0001 (Fig. 6b) (*19, 20*).

Obviously, the structure of the D$^+$ chromatophore could not be deduced from this simple spectrum alone. The most likely structure for the D$^+$ chromatophore is that of the bacteriochlorophyll a radical cation (BChl$^+$ a), the ESR spectrum of which is also shown in Fig. 6b (*21*). This radical, produced by oxidation in vitro, gave a single ESR line similar in shape and *g* value to that from the D$^+$ chromatophore except that ΔB was 13.0 ± 2.0 gauss. The proposed explanation for this unexpected difference in line width was that the $BChl^+$ a radical dimerized in vivo (*22*), an explanation confirmed by powder ENDOR studies of the systems in vivo and in vitro (*23, 24*).

As shown in Fig. 6c, three pairs of lines from three different kinds of protons were observed in both cases. The ENDOR lines were centered at the free proton frequency, but the hyperfine splittings calculated for the D^+ chromatophore were exactly half those obtained from $BChl^+$ a. This was consistent with the interpretation that, in the sample in vivo, the unpaired electron is shared equally between two $BChl^+$ a moieties, and thus the spin density and the hyperfine splittings from each proton are halved.

The actual assignment of the splittings to specific proton positions within the $BChl^+$ a molecule was more difficult. It was accomplished by first arguing that β protons in methyl groups would give sharp, intense ENDOR lines because rotational motion would average the anisotropic hyperfine interactions of the protons. The β protons not located in methyl groups would have weakly anisotropic hyperfine interactions and would give rise to broad, but relatively strong, signals. Finally, α and γ protons, with their highly anisotropic hyperfine interactions, would produce broad, weak ENDOR lines that would likely escape detection.

By this line of reasoning, all the proton ENDOR signals in Fig. 6c were assigned to β protons, the broad lines (C) being assigned to the four β protons in rings II and IV (Fig. 6a); this assignment was confirmed by selective-deuteration experiments (*25*). The line pairs A and B arise from β protons in the rotating methyl groups of rings I and III, respectively, with the distinction between the rings being made by comparison of ENDOR spectra from several types of well-characterized chlorophylls (*19*). All of these assignments were substantiated by solution ENDOR studies of $BChl^+$ a in a mixture of CH_2Cl_2 and CH_3OH (Fig. 6d) (*26, 27*). In solution, rotational averaging allowed the detection of signals from α and γ protons, in addition to the β protons observed by powder ENDOR.

In the above example, a specific question regarding intermolecular interactions was answered by powder ENDOR studies, and detailed information about the distribution of charge in a biologically important molecule was deduced from a combination of ENDOR spectroscopy and isotopic chemical substitution. Such detailed interpretations cannot always be made, but powder ENDOR spectra can still act as structural fingerprints that show differences between molecules not readily apparent from the ESR spectra alone.

Supplemental ENDOR techniques can also be used to simplify powder spectra. In one technique, circularly polarized ENDOR (CP-ENDOR), right or left circularly polarized rf fields are used to excite certain ENDOR transitions selectively (*28, 29*) (Fig. 5a).

Another supplemental technique that can be applied to both powders and crystals is polarization-modulated ENDOR (PM-ENDOR) (*28, 30*). For an ENDOR signal with maximum intensity, the rf field must be oriented perpendicular to B_0. PM-ENDOR makes use of the fact that the signal intensity can also depend on the orientation of B_2 in the plane (xy) perpendicular to B_0. Thus, if the direction of B_2 is rotated in the xy plane at a frequency of ν_2 (polarization-modulated), the intensity and the phase of the ENDOR signal will vary with the same frequency and can be monitored with phase-sensitive detection. The resultant PM-ENDOR signal will be smallest for nuclei with small or isotropic hyperfine couplings.

PM-ENDOR can be a useful technique for studying solids because it will discriminate against matrix ENDOR lines. These are strong resonance signals, located at the free nuclear frequency, that result from weak dipolar couplings between the unpaired electron and the distant nuclei in the sample (*1*) and that often obscure more informative ENDOR transitions. The phase relationship between the lines in a PM-ENDOR spectrum can be used to identify signals from the same nucleus and to give some information about the symmetry of the associated hyperfine interaction tensor (Fig. 5c).

Thus, by using a combination of elaborate modulation and multiple resonance schemes with isotopic enrichment and spectral simulation techniques, one can obtain a great deal of information from powder ENDOR spectra. Until now, most powder studies have been confined to organic and biological systems, in part because of the greater difficulty in obtaining single crystals of these materials, and in part because the conditions that complicate powder studies (the presence of abundant magnetic nuclei, large **g** and **A** anisotropies, and strong delocalization of unpaired electron spins) commonly occur in inorganic solids. Powder ENDOR studies of inorganic systems will probably assume more importance as interest in amorphous semiconductors increases and improvements in ENDOR techniques continue to be made.

Sensitivity is often a problem in ENDOR studies of powders as well as of single crystals that contain low paramagnetic defect concentrations. Recent developments in instrumentation, data acquisition, and filtering techniques have greatly improved the sensitivity of the technique (*8, 9*).

A major advance also has occurred with the advent of optically detected magnetic resonance (ODMR) (*31*). Here, ESR and ENDOR processes are detected through the modulation of optical emission and absorption transitions by microwave and rf fields. Techniques such as optically detected ESR (OD-ESR) and optically detected ENDOR (OD-ENDOR) provide information about both the ground and optically excited states of paramagnetic species. The potential of ODMR for studying defects in crystalline semiconductors, in which spin concentrations are generally low, has been demonstrated (*32, 33*). Its value in studying amorphous materials is also promising (*34*), even though line broadening exacerbates the problem of signal detection from practical concentrations of paramagnetic centers.

Finally, pulsed ENDOR (or spin-echo ENDOR), like ODMR, does not use the change in the ESR signal intensity as the detection channel for the ENDOR process. Instead, the ENDOR effect is detected by means of rf-induced changes in the relaxation characteristics of the electronic spin system. The principal advantage of pulsed ENDOR is that it does not depend on a delicate balance of nuclear and electronic relaxation times, and so it can often be used in cases in which ordinary ENDOR processes produce weak or undetectable signals (*35*).

References and Notes

1. L. Kevan and L. D. Kispert, *Electron Spin Double Resonance Spectroscopy* (Wiley, New York, 1976).
2. M. M. Dorio and J. H. Freed, Eds., *Multiple Electron Resonance Spectroscopy* (Plenum, New York, 1979).
3. *Electron Spin Resonance* (Royal Society of Chemistry, London, 1973–84), vols. 1–9.
4. K. Mobius and M. Plato, *Phys. Rep.* **87**, 171 (1982).
5. M. Plato, W. Lubitz, K. Mobius, *J. Phys. Chem.* **85**, 1202 (1981).
6. J. H. Freed, in *Multiple Electron Resonance Spectroscopy*, M. M. Dorio and J. H. Freed, Eds. (Plenum, New York, 1979), p. 73.
7. K. P. Dinse, R. Biehl, K. Mobius, *J. Chem. Phys.* **61**, 4335 (1974).
8. J. R. Niklas, "Elektronen-kern-doppelresonanz-spectroskopie zur strukturunter-suchung von festkörperstörstellen," thesis, Universität-GH Paderborn (1983).
9. ——, *Radiat. Eff.* **72**, 39 (1983).
10. M. T. Olm, J. R. Niklas, J.-M. Spaeth, M. C. R. Symons, in preparation.
11. T. H. James, Ed., *The Theory of the Photographic Process* (Macmillan, New York, 1977).
12. R. Biehl, M. Plato, K. Mobius, *J. Chem. Phys.* **63**, 3515 (1975).
13. J. S. Hyde, *ibid.* **43**, 1806 (1965).
14. J. M. Spaeth and J. R. Niklas, in *Recent Developments in Condensed Matter Physics*, J. T. DeVereese, Ed. (Plenum, New York, 1981), vol. 1, pp. 393–414.

15. L. R. Dalton and A. L. Kwiram, *J. Chem. Phys.* **57**, 1132 (1972).
16. B. M. Hoffman, J. Martinsen, R. A. Venters, *J. Magn. Reson.* **59**, 110 (1984).
17. G. C. Hurst, "Theory and applications of powder ENDOR: Observations and implications of asymmetry in proton powder ENDOR spectra of copper complexes," thesis, University of Rochester (1984).
18. A. J. Hoff, *Biophys. Struct. Mech.* **8**, 107 (1982).
19. B. Commoner, J. J. Heise, J. Townsend, *Proc. Natl. Acad. Sci. U.S.A.* **42**, 710 (1956).
20. P. Sogo, M. Jost, M. Calvin, *Radiat. Res. Suppl.* **1**, 511 (1959).
21. J. D. McElroy, G. Feher, D. C. Mauzerall, *Biochim. Biophys. Acta* **267**, 363 (1972).
22. J. R. Norris, R. A. Uphaus, H. L. Crespi, J. J. Katz, *Proc. Natl. Acad. Sci. U.S.A.* **68**, 625 (1971).
23. G. Feher, A. J. Hoff, R. A. Isaacson, J. D. McElroy, *Biophys. Soc. Abstr.* (1973), p. 61a.
24. J. R. Norris, M. E. Druyan, J. J. Katz, *J. Am. Chem. Soc.* **95**, 1680 (1973).
25. G. Feher, A. J. Hoff, R. A. Isaacson, L. C. Ackerson, *Ann. N.Y. Acad. Sci.* **244**, 239 (1975).
26. D. C. Borg, A. Forman, J. Fajer, *J. Am. Chem. Soc.* **98**, 6889 (1976).
27. A. J. Hoff and K. Mobius, *Proc. Natl. Acad. Sci. U.S.A.* **75**, 2296 (1978).
28. A. Schweiger, *Struct. Bonding (Berlin)* **51**, 1 (1982).
29. ——— and Hs. H. Gunthard, *Mol. Phys.* **42**, 283 (1981).
30. ———, *J. Magn. Reson.* **57**, 65 (1984).
31. J. J. Davies, *Contemp. Phys.* **17**, 275 (1976).
32. B. K. Meyer, J.-M. Spaeth, M. Scheffler, *Phys. Rev. Lett.* **52**, 851 (1984).
33. D. M. Hofmann, B. K. Meyer, F. Lohse, J.-M. Spaeth, *ibid.* **53**, 1187 (1984).
34. Y. Sano, K. Morigaka, I. Hirabayashi, *Physica B* **117-118**, 923 (1983).
35. W. B. Mims, in *Fourier, Hadamard, Hilbert Transforms in Chemistry*, A. G. Marshall, Ed. (Plenum, New York, 1982), pp. 307–322.

Slow Neutron Scattering Experiments

Ralph M. Moon

Summary. Neutron scattering is a versatile technique that has been successfully applied to condensed-matter physics, biology, polymer science, chemistry, and materials science. The United States lost its leadership role in this field to Western Europe about 10 years ago. Recently, a modest investment in the United States in new facilities and a positive attitude on the part of the national laboratories toward outside users have resulted in a dramatic increase in the number of U.S. scientists involved in neutron scattering research. Plans are being made for investments in new and improved facilities that could return the leadership role to the United States.

Neutron scattering has undergone dramatic worldwide growth over the last decade. This growth has occurred in both the number of practitioners and the number of scientific disciplines in which neutron scattering has been productively applied. The trigger responsible for this activity was the success of the Institut Laue-Langevin (ILL) in Grenoble, France. Largely because of ILL, where intense neutron beams, innovative instrumentation, and institutional policies have combined to create a great interest in and demand for neutron scattering facilities, the leadership in this field has shifted from the United States to Western Europe.

This article describes the scientific diversity of neutron scattering, discusses the growth of the U.S. neutron scattering community, and reviews plans for restoring the United States to a position of leadership in this important field. These topics have been the subject of several recent review articles and national discussions about the application of neutron scattering to condensed-matter physics (*1*), biology (*2*), and polymer science (*3*); about ILL and other European activities (*4*); about pulsed neutron sources (*5, 6*); about instrumentation at reactors (*7*); and about the present status of and future plans for neutron scattering in the United States (*8, 9*).

Fundamental Properties of the Neutron

The growth of neutron scattering is firmly rooted in certain fundamental properties of the neutron that impart to it some unique advantages over other commonly used scattering probes. Some characteristics of neutrons, x-rays, and electrons, all with a wavelength of 1 Å, are given in Table 1. For structural studies, in which the goal is to determine the relative positions of atoms within the sample, a probe with wavelength comparable to interatomic distances is desired. Clearly all three probes can be used for structural determinations, with the selection of the most appropriate probe resting on factors other than wavelength. For dynamic studies, in which the goal is to determine the relative motions of atoms within the sample, it is desirable to have a probe with energy comparable to the energy of motion of the atoms in the sample. Because thermally activated motions have energies generally less than 100 meV, the neutron has a great natural advantage for studies of the dynamics of condensed matter.

The relatively slow velocity of thermal neutrons means that easily measured flight times of the order of milliseconds are obtained for distances of a few meters. Thus, time-of-flight techniques are an important part of the total experimental picture in neutron scattering.

There are three important points to be made with regard to neutron scattering amplitudes compared to those of x-rays and electrons. First, the fact that neutrons are relatively weakly interacting (as shown in Table 1) means that multiple scattering effects are less important for neutrons and that measured macroscopic cross sections are more easily interpreted. Second and most important, the nuclear scattering amplitudes for neutrons do not vary systematically across the periodic table as do the corresponding amplitudes for x-rays and electrons. This has important consequences for the ability of neutrons to "see" light atoms in the presence of heavy atoms and to distinguish between neighboring atoms in the periodic table. There is even strong variation in scattering amplitude among isotopes of the same element. The hydrogen-deuterium case is particularly important and is discussed later in connection with applications to biology and polymer science. Finally, the fact that the nuclear interaction between neutrons and nuclei is short range means that the nuclear scattering is isotropic for slow neutrons; there is no form factor as there is in the x-ray case. This has two

---

R. M. Moon is a member of the Solid State Division, Oak Ridge National Laboratory, Oak Ridge, Tennessee 37831.